

# Atomically Thin Layers of Graphene and Hexagonal Boron Nitride Made by Solvent Exfoliation of Their Phosphoric Acid Intercalation Compounds

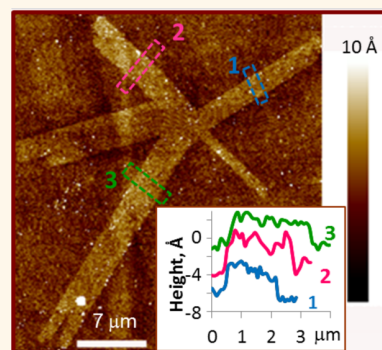
Nina I. Kovtyukhova,<sup>†,‡</sup> Nestor Perea-López,<sup>§</sup> Mauricio Terrones,<sup>‡,§</sup> and Thomas E. Mallouk<sup>\*,‡,§,||</sup>

<sup>†</sup>Departments of Chemistry, <sup>§</sup>Physics, and <sup>||</sup>Biochemistry and Molecular Biology, The Pennsylvania State University, University Park, Pennsylvania 16802, United States

**S** Supporting Information

**ABSTRACT:** The development of scalable and reliable techniques for the production of the atomically thin layers of graphene and hexagonal boron nitride (h-BN) in bulk quantities could make these materials a powerful platform for devices and composites that impact a wide variety of technologies (*Nature* 2012, 490, 192–200). To date a number of practical exfoliation methods have been reported that are based on sonicating or stirring powdered graphite or h-BN in common solvents. However, the products of these experiments consist mainly of few-layer sheets and contain only a small fraction of monolayers. A possible reason for this is that splitting the crystals into monolayers starts from solvent intercalation, which must overcome the substantial interlayer cohesive energy (120–720 mJ/m<sup>2</sup>) of the van der Waals solids. Here we show that the yield of the atomically thin layers can be increased to near unity when stage-1 intercalation compounds of phosphoric acid are used as starting materials. The exfoliation to predominantly monolayers was achieved by stirring them in medium polarity organic solvents that can form hydrogen bonds. The exfoliation process does not disrupt the sp<sup>2</sup>  $\pi$ -system of graphene and is gentle enough to allow the preparation of graphene and h-BN monolayers that are tens of microns in their lateral dimensions.

**KEYWORDS:** graphite, boron nitride, graphene, intercalation, exfoliation, nanosheets



Liquid-phase processing of atomically thin sheets derived from layered solids (as well as many other nanomaterials) is an economical, scalable and convenient way to produce them in bulk quantities, in order to fabricate different types of heterostructures, composites, and devices. Single-step deposition from solutions offers the advantages of using substrates of different chemical compositions and shapes. This flexibility facilitates the characterization of monolayers and broadens their possible applications. Because of their the electronic and thermal properties that derive from their 2D structure, their chemical stability, and very high surface to volume ratio, monolayers of graphene and hexagonal boron nitride (h-BN) could become components of electronic and photonic devices (including flexible ones), transparent electrodes, smart coatings, composites, membranes, energy generation and storage devices, sensors, and biosensors<sup>1–3</sup> once rapid, scalable and reliable methods for their production are developed.

There are a number of examples of successful exfoliation of graphite and h-BN by sonicating and/or stirring the powders in

common solvents,<sup>4–8</sup> and the criteria for selecting “good” solvents have been developed using the theory of Hansen solubility parameters (HSP). However, the exfoliated product resulting from these methods is dominated by multilayer graphene and h-BN sheets and only small amounts of monolayers are present. One of the reasons for this may be found in the crystalline structure of the starting layered crystals. As shown in Figure 1a,b, microcrystalline platelets of graphite and h-BN, which are typically hundreds of nanometers to microns thick, consist of stacks of much thinner densely packed slabs. Their segmented structure represents the disruption of atomically coherent stacking along the crystallographic *c*-axis, which may be caused by shear and basal dislocations, and by the presence of twist grain boundaries.<sup>9</sup> In our studies of graphite and h-BN intercalation by nonoxidizing Brønsted acids, we found that the intercalation process began with the

**Received:** February 23, 2017

**Accepted:** July 7, 2017

**Published:** July 7, 2017

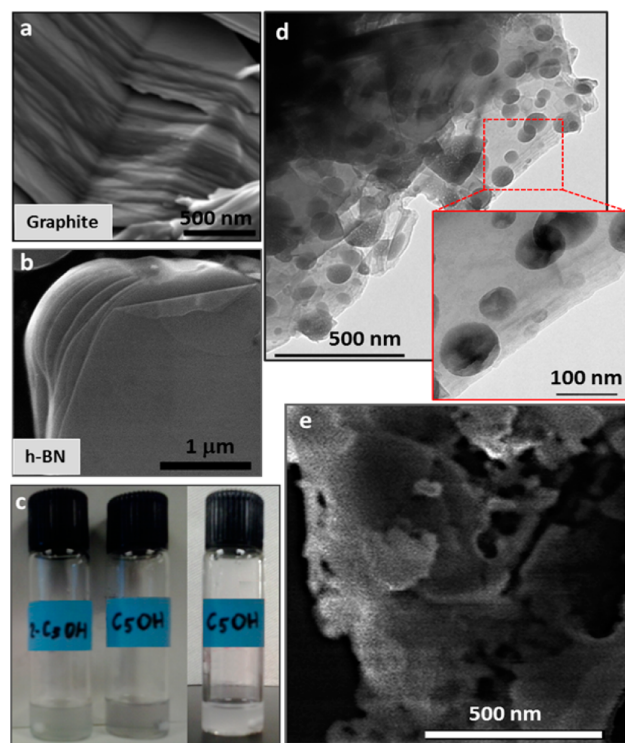


**Figure 1.** (a, b) SEM images of graphite (a) and h-BN (b) crystals of the starting powders show the edges of the crystals that are composed of densely packed slabs. (c) Photographs of dispersions of the exfoliated graphite/ $\text{H}_3\text{PO}_4$  (left) and BN/ $\text{H}_3\text{PO}_4$  (right) in pentanol and isopropanol. (d, e) TEM and SEM images of partially exfoliated graphite/ $\text{H}_3\text{PO}_4$  crystals in *i*-PrOH: (d) shows flat  $\text{H}_3\text{PO}_4$  agglomerates leaving the interlayer galleries (overlap of the agglomerate images indicates their positioning between different layers across the graphite crystal); (e) depicts formation of cracks, holes and some disintegration of the larger graphite particles during intercalation/exfoliation.

relatively fast separation of these few-nm-thick slabs, followed by slower conversion to stage-1 intercalation compounds.<sup>10,11</sup> Similar observations have been reported in the oxidation and thermal expansion of graphite.<sup>9</sup> It is reasonable to expect that exfoliation with organic liquids might also begin by splitting the parent microcrystals at these weak links into slabs (*i.e.*, multilayer sheets), which in some cases become the final product after exfoliation. The small difference between the surface energies of the slabs and solvents facilitates the exfoliation process.<sup>4,5</sup> However, splitting the slabs into monolayers involves solvent intercalation, which presumably begins at the edges and must overcome the interlayer cohesive energy ( $120\text{--}720\text{ mJ/m}^2$ ).<sup>12–19</sup> The strength of the van der Waals interaction between sheets in fact grows progressively with thinning of the multilayer slabs.<sup>20</sup> This makes the complete intercalation by organic solvents energetically unfavorable (or at least very slow under mild conditions), and it is a possible reason for finding a small fraction of monolayers in the solvent exfoliation of graphite and h-BN.

In the case of the stage-1 intercalation compounds (ICs), we begin with graphene and h-BN layers that are already separated by Brønsted acid molecules. The intercalation of these molecules reduces the interlayer cohesive energy and facilitates exfoliation to the atomic layers,<sup>10,21</sup> but requires the selection of a solvent with optimal affinity for both the host and guest

components. This may not be a trivial task since literature data on the surface energies of graphite and h-BN powders are rather scarce and vary in the ranges of several tens of units,<sup>12–19,23–25</sup> and since HSPs for these materials are yet to be determined.<sup>5</sup> Furthermore, the surface properties of host monolayers that have been in contact with acid molecules can differ from those of the intact host crystals and thus require separate characterization.

Here we demonstrate that exfoliation of the phosphoric acid intercalation compounds of graphite and h-BN to yield predominantly monolayers is achievable by using medium polarity organic solvents that are capable of forming hydrogen bonds. This intercalation/exfoliation process is not destructive and monolayers that are tens of microns in their lateral dimensions can be obtained.

## RESULTS AND DISCUSSION

**Selection of Solvents.** The process of exfoliating  $\text{H}_3\text{PO}_4$ -intercalated graphite and h-BN involves a number of steps: (i) *wetting of the acid-covered crystals by the solvent*, which should be considered a separate step because  $\text{H}_3\text{PO}_4$  forms a relatively thick coating around the crystals (Figure S1), and its dissolution provides solvent access to the surface of the microcrystals, (ii) *interaction of the solvent with guest acid molecules to extract them from the interlayer galleries*, and simultaneously, interaction of the solvent molecules with the host layers—the solvent-sheet interaction should be strong enough to penetrate the gradually vacated galleries to cause exfoliation (*i.e.*, prevent restacking of the host crystal layers), and (iii) *dispersion of the exfoliated layers in the solvent* to give relatively stable and manageable suspensions. This suggests that a good solvent should have strong affinity for both the polar  $\text{H}_3\text{PO}_4$  molecules and the nonpolar graphene and h-BN surfaces.

Indeed, our preliminary experiments showed that nonpolar liquids, such as hexane and toluene, did not wet the  $\text{H}_3\text{PO}_4$  intercalation compounds and hence no dispersion/exfoliation occurred. On the other hand, high polarity solvents, such as dimethyl sulfoxide (DMSO) and *N*-methyl-2-pyrrolidone (NMP), are good dispersants for both of the intercalation compounds, but they destroy graphene and h-BN monolayers (*i.e.*, TEM shows large shapeless holey film pieces in the DMSO solutions and no significant amount of solid particles in the transparent solutions in NMP even at room temperature). Water was also excluded from this study because it was shown to introduce defects into graphene sheets,<sup>21</sup> and it is also likely to promote hydrolysis of h-BN monolayers,<sup>8</sup> especially in the presence of  $\text{H}_3\text{PO}_4$ .

To select minimally corrosive solvents that have a strong interaction with both guest and host components of the intercalation compounds, we mainly considered two observations: first, both of the components, graphene and h-BN sheets,<sup>10,11</sup> and  $\text{H}_3\text{PO}_4$ , have a common tendency to interact with acidic OH hydrogen atoms to form hydrogen bonds, and second, oxygenated alkane derivatives readily assemble on the graphite surface.<sup>22</sup> Therefore, we studied several common protic solvents of medium polarity and different alkyl chain lengths: isopropanol (*i*-PrOH), *n*-pentanol ( $\text{C}_5\text{OH}$ ), 3-octanol ( $3\text{-C}_8\text{OH}$ ) and *n*-octanoic acid ( $\text{C}_8\text{OOH}$ ), and the aprotic solvent dimethylformamide (DMF) that was previously found to be a good dispersant for graphite/ $\text{H}_3\text{PO}_4$ <sup>10</sup> and h-BN.<sup>5</sup>

**Exfoliation.** First-stage graphite/ $\text{H}_3\text{PO}_4$  and BN/ $\text{H}_3\text{PO}_4$  intercalation compounds that contained some amount of the

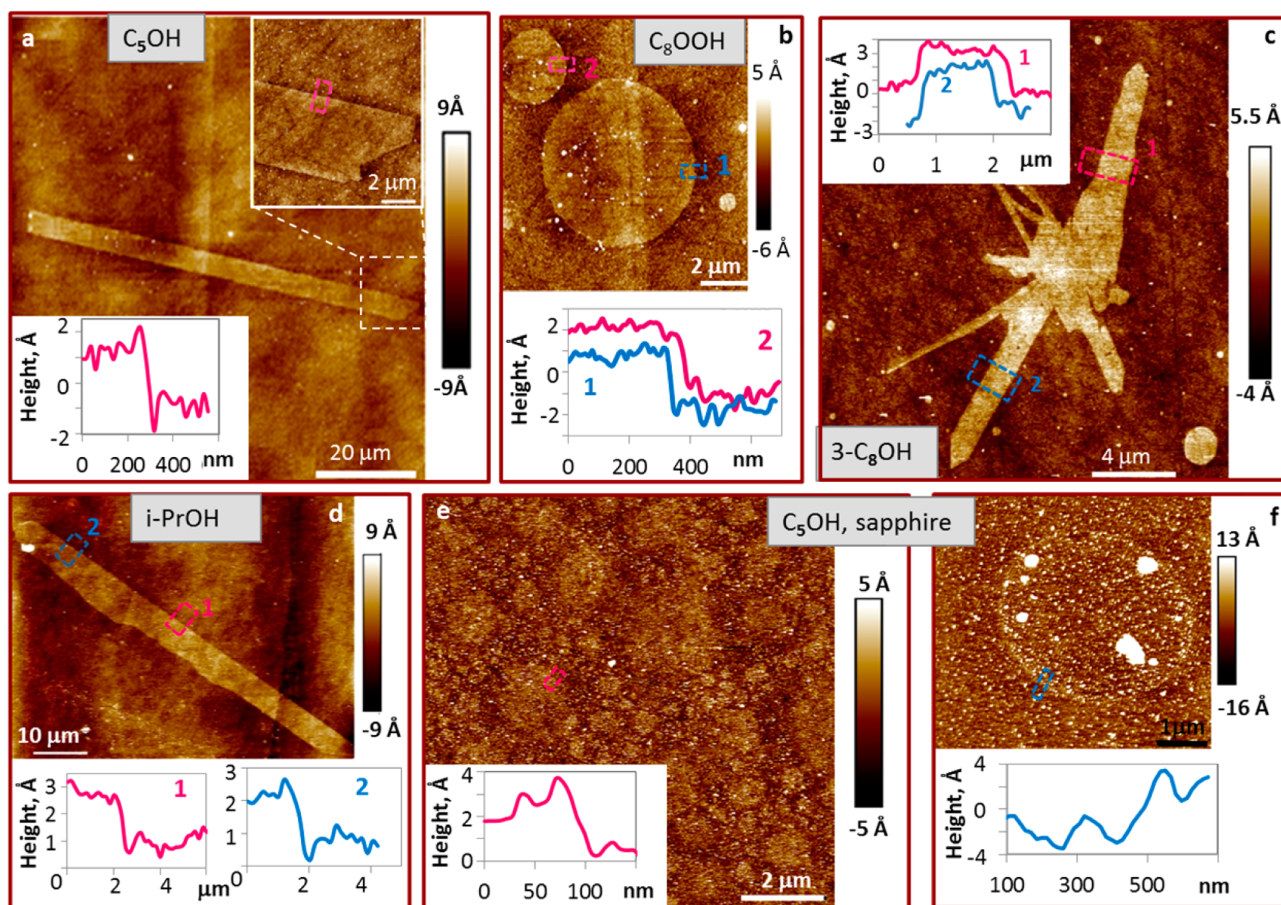


**Figure 2.** AFM images illustrate graphite/ $\text{H}_3\text{PO}_4$  exfoliation in polar solvents. (a–d) Large monolayer cryo-milled graphite (CMG) sheets on Si substrate that occur in all solvents under investigation. (e, f) CMG (e) and natural graphite powder (GAK-2, Ukraine, 325 mesh) (f) monolayers on a sapphire substrate. Relatively densely packed graphene monolayers can be found in some places on the sapphire surface, however the more polar surface causes occlusion of the solvent under the monolayers. Insets in (a–f) show height (2–3 Å) of the graphene sheets consistent with graphene monolayer thickness; height measurement areas are indicated by pink and blue boxes on the images.

intact host crystals (see XRD patterns in Figure S1) were dispersed in the solvents listed above by stirring. This resulted in the formation of light gray (graphite) and milky white (h-BN) slightly opalescent homogeneous suspensions. At room temperature this process takes  $\sim 1$  h with DMF and *i*-PrOH,  $\sim 6$  h with  $\text{C}_5\text{OH}$ , and 2+ days with  $3\text{-C}_8\text{OH}$  and  $\text{C}_8\text{OOH}$ . In the latter case some large particles are always observable. These particles are most likely agglomerates of the poorly wetted  $\text{H}_3\text{PO}_4$  acid-covered intercalation compounds as well as intact h-BN or graphite microcrystals. We note that, unlike relatively fluffy microcrystalline powders of bare graphite and h-BN, the intercalation compounds exist as larger, hard crystalline agglomerates that are bound together by their acid-covered surfaces (Figure S1), and thus their dispersion in the same solvents is slower. Increasing the temperature to  $60^\circ\text{C}$  (DMF, *i*-PrOH and  $\text{C}_5\text{OH}$ ) and to  $120^\circ\text{C}$  ( $3\text{-C}_8\text{OH}$  and  $\text{C}_8\text{OOH}$ ), significantly accelerates the wetting process and homogeneous suspensions form within minutes with DMF, *i*-PrOH and  $\text{C}_5\text{OH}$  and within several hours with  $3\text{-C}_8\text{OH}$  and  $\text{C}_8\text{OOH}$  (although a few large particles are still visible in the case of  $\text{C}_8\text{OOH}$ ). This is consistent with a decrease in solvent viscosity at higher temperature, which facilitates wetting/dissolution of the  $\text{H}_3\text{PO}_4$  coating and dispersion of crystals of the intercalation compounds (see SI p 2 for more details).

We assume that the outer acid coating is washed away as soon as the homogeneous suspensions form, and intercalated  $\text{H}_3\text{PO}_4$  becomes accessible to the solvent, which initiates the exfoliation of graphite/ $\text{H}_3\text{PO}_4$  and h-BN/ $\text{H}_3\text{PO}_4$  crystals. Figure 1d shows such a “washed,” partially exfoliated crystal as  $\text{H}_3\text{PO}_4$  leaves the expanded interlayer galleries. As the exfoliation progresses, the suspensions of graphite/ $\text{H}_3\text{PO}_4$  and h-BN/ $\text{H}_3\text{PO}_4$  become almost transparent birefringent sols (Figure 1c) that are relatively stable (*i.e.*, no precipitation is noticeable during 2–3 h).

AFM analysis shows that exfoliation of the graphite/ $\text{H}_3\text{PO}_4$  and h-BN/ $\text{H}_3\text{PO}_4$  intercalation compounds results in the formation of mostly monolayer (2–3.5 Å high) and bilayer (4–7 Å high) graphene and h-BN sheets together with smaller amounts of few-layer crystals. Figures 2 and 3 display images of monolayer graphene and h-BN sheets prepared in *i*-PrOH,  $\text{C}_5\text{OH}$ ,  $\text{C}_8\text{OOH}$ , and  $3\text{-C}_8\text{OH}$  (for similar graphene monolayers prepared in DMF, see ref 10). TEM analysis shows that the graphene<sup>10</sup> and h-BN (Figure 3a) monolayer sheets are single crystals with no noticeable morphological damage.

In both the graphite/ $\text{H}_3\text{PO}_4$  and BN/ $\text{H}_3\text{PO}_4$  systems, the monolayer fraction consists mainly of sheets with small lateral dimensions ( $<100\text{--}500$  nm) and some amount of larger (0.5–3  $\mu\text{m}$ ) sheets (see monolayer distribution by lateral dimensions in Figure S3). However, monolayers as large as 10–80  $\mu\text{m}$  can

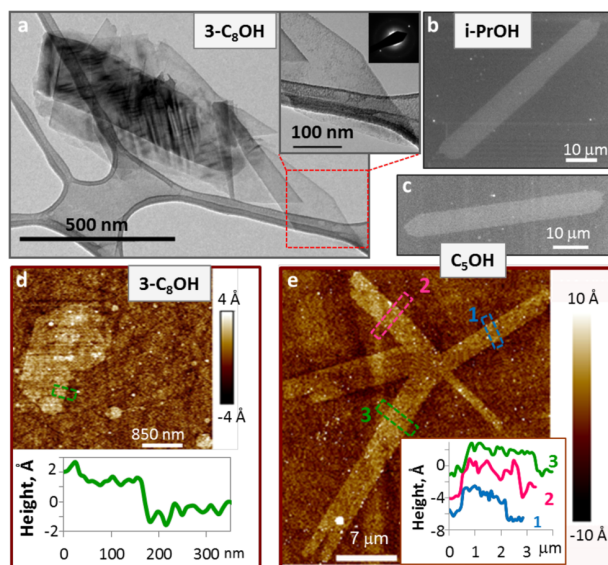


**Figure 3.** TEM (a), FESEM (b, c) and AFM (d, e) images of h-BN/ $\text{H}_3\text{PO}_4$  exfoliated to monolayers in 3- $\text{C}_8\text{OH}$  (a, d), *i*-PrOH (b) and  $\text{C}_5\text{OH}$  (c, e) and deposited on Si[100] substrates (b–e). (a) Few-layer scroll and single crystal monolayer sheet with SAED pattern (inset). Insets in (d) and (e) show height (2–3 Å) of the h-BN sheets consistent with the monolayer thickness; height measurement areas indicated by pink green and blue boxes on the images.

also be found in all of the solvents except DMF (Figures 2, 3). It appears that in less polar solvents with longer alkyl chains, especially  $\text{C}_8\text{OOH}$ , the proportion of the larger monolayer sheets is higher, whereas in the most polar solvent, DMF, we have not found monolayers larger than  $1\ \mu\text{m}$  (Figure S3). Using higher exfoliation temperatures in DMF we do observe monolayers with lateral dimensions of  $\sim 3\ \text{mm}$ , but they all are morphologically damaged (Figure S4). With *i*-PrOH,  $\text{C}_5\text{OH}$ ,  $\text{C}_8\text{OOH}$ , and 3- $\text{C}_8\text{OH}$  as solvents, the lateral size of the monolayers is most likely determined by the crystal quality of the starting graphite and h-BN powders. Because monolayers with lateral dimensions comparable to those of the parent microcrystals (1–100  $\mu\text{m}$ ) are found in all solvents except DMF, it appears that the intercalation/exfoliation process is gentle enough to preserve the crystalline integrity of the monolayers.

Indeed, Raman spectra (Figure 4 and Figure S5a–c) show that intercalation/exfoliation procedure does not damage the  $\text{sp}^2$   $\pi$ -electron system of exfoliated graphene or h-BN and does not introduce a noticeable amount of  $\text{sp}^3$  defects which might promote monolayer disintegration.

On the other hand, it has been shown that individual crystal flakes are typically stacks of fairly randomly shaped and arranged polygons that contain multiple layers.<sup>9</sup> SEM images of the starting graphite and h-BN powders (insets in Figure S3) support this polygonal flake model of the structure. Therefore, in addition to the contribution of initially small particles, larger polygonal crystals can break apart during the intercalation and/or exfoliation processes to give small single- or few-layer sheets, significantly increasing the fraction of monolayers with small lateral dimensions. Indeed, SEM images of partially exfoliated graphite/ $\text{H}_3\text{PO}_4$  particles show cracks and holes in many of the crystals (Figure 1e). The microstructure of crystalline graphite is known to depend strongly on the crystal growth conditions, and this should substantially impact results obtained with

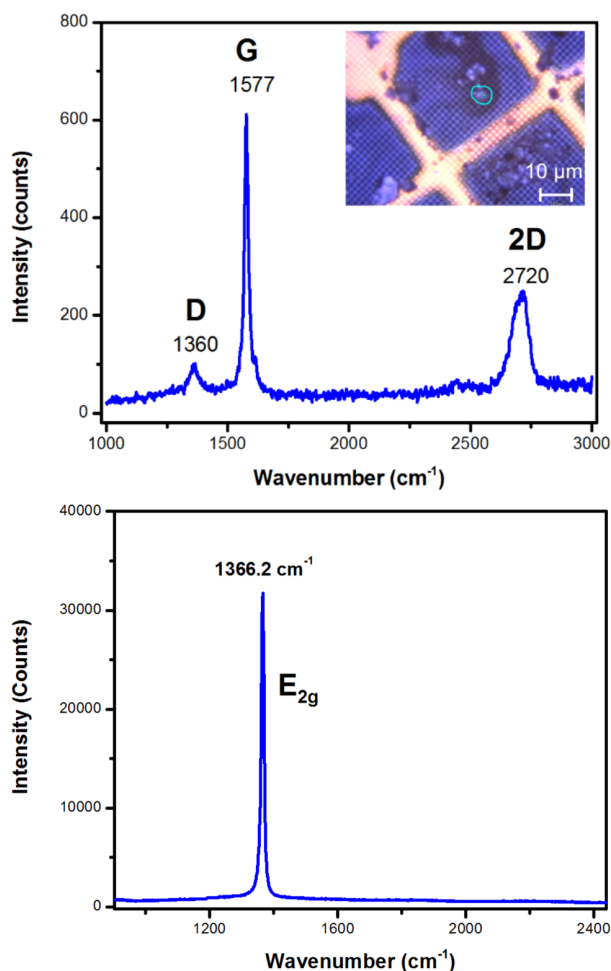


**Figure 4.** (Top) Raman spectrum collected from an agglomerate of restacked graphene sheets, which may contain mono- and few-layer graphene, drop cast onto a Quantifoil TEM grid (inset). The excitation wavelength was 514.5 nm, the spectrometer was a Renishaw inVia microRaman using a 100 $\times$  objective with a 0.95 numerical aperture. (Bottom) Raman spectrum of a h-BN sheet cast on a silicon substrate, showing the characteristic in-plane vibrational mode ( $\text{E}_{2g}$ ) of h-BN at  $1366.2\ \text{cm}^{-1}$ . The spectral acquisition was done in a Horiba LabRam HR Evolution UV Raman Spectrometer using a 74 $\times$  UV objective and a 290 nm wavelength laser excitation.

different graphite powders. For example, only very small graphene sheets resulted from the exfoliation of  $\text{SO}_3$  intercalation compounds prepared from synthetic graphite.<sup>21</sup>

The relative yields of monolayers and bilayers that are described below were obtained by analysis of 15–25 AFM images in each case. It is important to note here that quantitative AFM data on the fraction of monolayers and bilayers involve some uncertainty. They are statistical quantities derived from coverage densities of individual sheets, which were measured outside the drying rings, and do not necessarily reflect the distribution of sheets in the liquid suspensions. We also observe many h-BN and graphene sheets with lateral dimensions smaller than 70 nm, and these are ignored in estimating the monolayer and bilayer fractions. Relatively large particle agglomerates also form when drying drops of solution on the substrate and cannot be analyzed by AFM. Sometimes we also observe areas where the solvent is occluded under

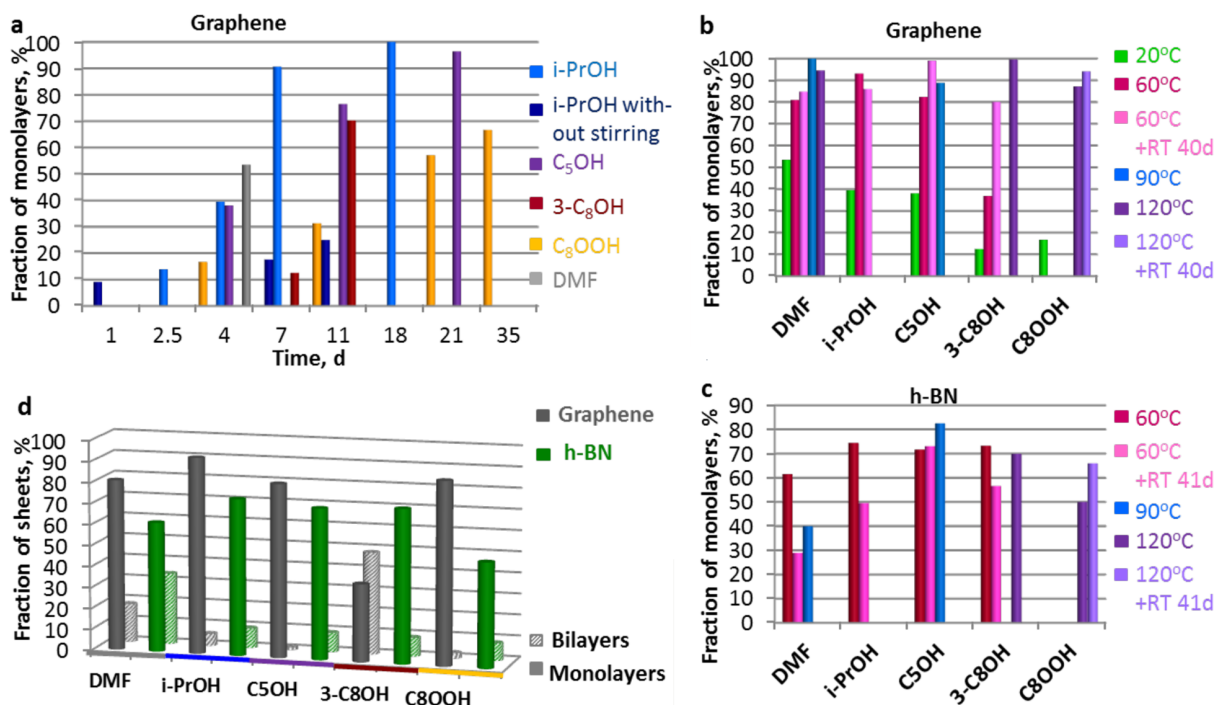


**Figure 5.** AFM analysis of monolayer and bilayer sheets yield after exfoliation of CMG/H<sub>3</sub>PO<sub>4</sub> and h-BN/H<sub>3</sub>PO<sub>4</sub> in polar solvents: time and temperature dependence. (a) Fraction of graphene monolayers vs time after exfoliation of CMG/H<sub>3</sub>PO<sub>4</sub> at ambient conditions. In *i*-PrOH exfoliation was studied with and without stirring (blue and dark blue, respectively). (b) Fraction of graphene monolayers after exfoliation of CMG/H<sub>3</sub>PO<sub>4</sub> at different temperatures for 2 days (at 20 °C: 4 d for all solvents and 7 d for 3-C<sub>8</sub>OH). (c) Fraction of h-BN monolayers after exfoliation of h-BN/H<sub>3</sub>PO<sub>4</sub> at different temperatures for 2 days. In (b) and (c) the suspensions exfoliated at 60 °C (120 °C in C<sub>8</sub>OOH) were allowed to stay at RT for 40–41d and analyzed by AFM again (pink and lilac, respectively). (d) Exfoliation CMG/H<sub>3</sub>PO<sub>4</sub> and h-BN/H<sub>3</sub>PO<sub>4</sub> at 60 °C for 2 days.

sheets, thus preventing precise measurements of the sheet height.

The yield of the monolayers depends on the temperature and the duration of the exfoliation process (Figure 4). At ambient temperature the exfoliation of graphite/H<sub>3</sub>PO<sub>4</sub> requires several days to complete. Larger, less polar solvent molecules (C<sub>8</sub>OOH, 3-C<sub>8</sub>OH, C<sub>5</sub>OH) work 2–3 times slower than smaller solvent molecules (*i*-PrOH and DMF) (Figure 5a). Exerting shear force (by stirring, not sonication) significantly accelerates exfoliation of bare graphite,<sup>6</sup> and we observe a similar effect with the intercalation compounds (compare results for *i*-PrOH with and without stirring in Figure 5a). Increasing the temperature accelerates the exfoliation process by a factor of 2–10. At 60 °C (*i*-PrOH, DMF), 90 °C (C<sub>5</sub>OH) and 120 °C (C<sub>8</sub>OOH and 3-C<sub>8</sub>OH) exfoliation of both graphite/H<sub>3</sub>PO<sub>4</sub> and h-BN/H<sub>3</sub>PO<sub>4</sub> can be completed in ~2 days (Figure 5b,c). We judge the exfoliation process to be complete when the yield of the monolayers approaches 100% or there is no significant growth of the monolayer fraction after the suspensions are cooled to room temperature and allowed to stand for several days (see SI pp 4–5 and Figure S6 for more details).

When compared to h-BN/H<sub>3</sub>PO<sub>4</sub>, graphite/H<sub>3</sub>PO<sub>4</sub> gives a higher (by 10–30%) yield of monolayers under the same conditions in all solvents except 3-C<sub>8</sub>OH, which gives complete exfoliation of h-BN/H<sub>3</sub>PO<sub>4</sub> at 60 °C (Figure 5c,d). We note that in DMF at 90–120 °C, although the fraction of graphene monolayers slightly increases, morphological damage of the sheets can occur (Figure S4). This may be more pronounced for h-BN monolayers, the fraction of which significantly

decreases in DMF at 90 °C. In general, h-BN monolayers appear to be less stable than graphene because their fraction also decreases with time in DMF and *i*-PrOH even at ambient temperature (Figure 5c), and because smaller particles are more susceptible to degradation (Figure S3).

Increasing the temperature can accelerate the exfoliation process through both thermodynamic and kinetic effects in each exfoliation step (i–iii). Besides the energetic contribution to the dissolution of H<sub>3</sub>PO<sub>4</sub> (both the outer coating and then the deintercalated acid molecules, stages i–ii), higher temperatures can facilitate breaking bonds that formed due to the guest–host dipolar interactions in the intercalation process (stage ii),<sup>10,11</sup> increase the rate of diffusion of the acid/solvent molecules out of/into the interlayer galleries (stage ii), and also decrease the surface energy of the solvents that interact with the host layers (stages ii and iii). Assuming that dissolution of the outer acid coating is fast, the extraction of intercalated H<sub>3</sub>PO<sub>4</sub> and/or solvent diffusion into the galleries (stage ii) may be the rate-limiting step. This is consistent with longer exfoliation times and higher temperatures required for the larger solvent molecules with higher cohesion energy (Figure S2). In the subsequent stage (iii) of peeling apart and dispersing the host layers, the solvent molecules with longer alkyl tails should perform better than small molecules and do not require higher temperatures.

**Correlation of Exfoliation Yields with Solvent Parameters.** When comparing the highest yields of monolayers that result from complete exfoliation achievable with each solvent, one can see that the efficiency of the solvents studied decreases in the following order:



for graphite/ $H_3PO_4$  and



for h-BN/ $H_3PO_4$ .

For both of the intercalation compounds, alcohols perform slightly better than the carboxylic acid  $C_8OOH$ , and all the protic solvents are better than the aprotic solvent DMF (we do not consider data for DMF at 90–120 °C because of the uncertainty caused by decomposition of the monolayer sheets).

Plotting the monolayer fractions of graphene and h-BN *versus* energy of vaporization of the solvents and  $H_3PO_4$ , does not show any clear correlation (Figure 6a, top left).  $C_8OOH$ , which is the poorest solvent match for phosphoric acid (its  $DE_{vap}$  is  $\sim 11$  kJ/mol higher than the upper border of the  $DE_{vap}$  range for  $H_3PO_4$ ), is more efficient in exfoliating both of the intercalation compounds than DMF, which can dissolve the acid much faster (judging from the data in Figure 5a). This suggests that the efficient solvation of  $H_3PO_4$  is not a strong determinant in the final degree of exfoliation, but is an important factor at the preliminary stage of removal of the outer acid coating, which is necessary for the exfoliation process to begin.

Graphs of the monolayer fraction *versus* solvent surface energy (Figure 6a top right) reveal that higher exfoliation yields are observed for the solvents (the alcohols and octanoic acid) with surface energy in the range of 51–59  $mJ/m^2$  with a maximum of 56  $mJ/m^2$  for  $C_5OH$ . These data match well with values published in the literature of surface energies determined by contact angle measurements (44–66  $mJ/m^2$ )<sup>23</sup> and by the capillary rise method (25–60  $mJ/m^2$ )<sup>24</sup> for several h-BN and graphite/graphene (46–55  $mJ/m^2$ )<sup>25</sup> powders. The least effective solvent, DMF, has the highest surface energy. This correlation supports the idea that the interaction of solvent molecules with the host layers, rather than with guest acid molecules, determines the efficiency of the exfoliation process.

To better understand the nature of these interactions we further analyze our data within the theory of Hansen solubility parameters (HSP) that describe contributions of dispersive,  $d_D$ , polar,  $d_P$ , and hydrogen bonding,  $d_H$ , interactions to the total cohesive energy density.<sup>26</sup> It is commonly accepted that solvents capable of dispersing/dissolving solid powders are likely to have HSPs close to those of the solid (see SI pp 4–5 for details).

The five “good” solvents used in our study have relatively close values of HSPs (Table S1), and cannot be used to reliably assign HSPs to the graphene and h-BN monolayers. Therefore, we have attempted to find an analogue(s) among solids with a wide range of determined HSPs that show affinity for all five solvents similar to those of the graphene and h-BN monolayers. Therefore, we used the parameters of a group of ten carbon materials (Table S1)<sup>26</sup> and calculated the relative energy difference (RED) numbers for our five solvents (Figures 5b and S7, see SI pp 5–7 for details). In general,  $RED < 1$  indicates high solute affinity for a solvent, and the best solvent for a particular solute has the lowest RED number. Among the carbons that have  $RED < 1$  (Figure 5b) only carbon black CB1(t) has a set of RED numbers that qualitatively fits the order of exfoliation efficiency for all five solvents (*i.e.*, DMF and  $C_8OOH$  have higher RED numbers than alcohols with  $C_5OH$  having the lowest RED number). This suggests that the affinity of CB1(t) to all five solvents is close to that of the graphene

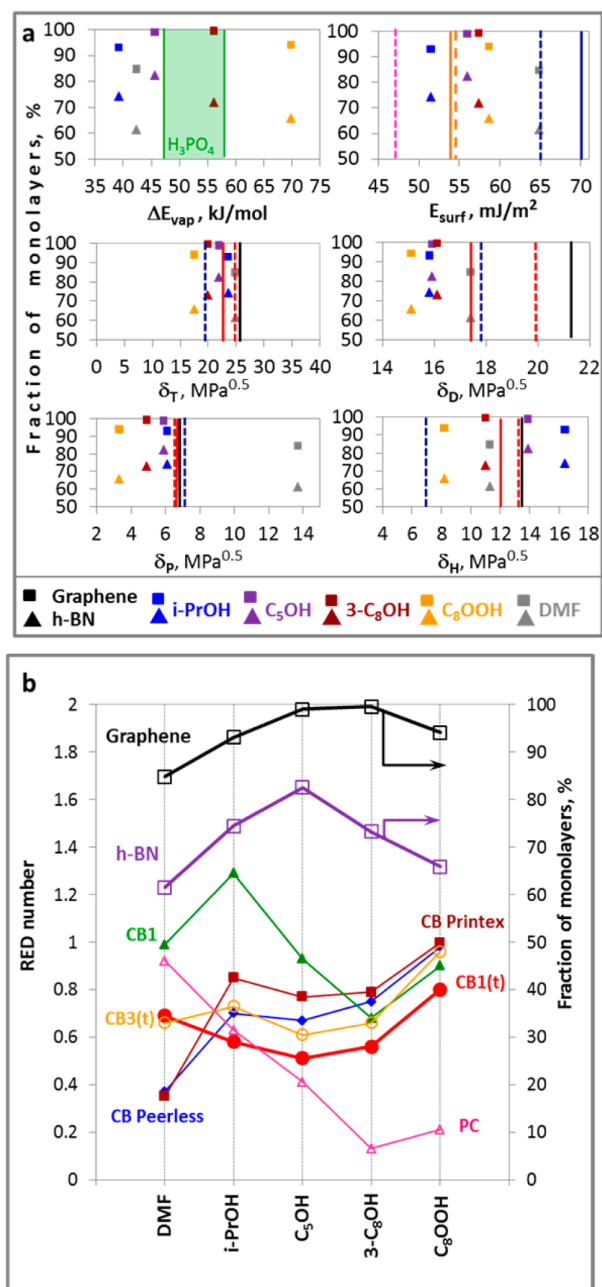


Figure 6. (a) Analysis of graphene (squares) and h-BN (triangles) monolayer yield dependence on total cohesive energy of the solvents (top left), surface energy of the solvents (top right) and Hansen solubility parameters (HSP),  $d$ , (middle-bottom). “D”, “P” and “H” indexes for  $d$  indicate dispersion, polarity and H-bonding components, respectively, of the total,  $d_T$ , solubility parameter. Top left: green area shows the range of total cohesive energies of  $H_3PO_4$  that correspond to the experimental conditions. Solvents energies are given for the temperatures at which the highest monolayer yields were achieved (60 °C, DMF and  $i$ -PrOH; 90 °C,  $C_5OH$ ; 120 °C,  $3-C_8OH$  and  $C_8OOH$ ); solvents HSPs are for 25 °C.<sup>26</sup> Vertical lines on the graphs: Dashed lines, literature data for corresponding energies and HSPs for h-BN (blue,<sup>5</sup> orange and pink, middle of the energy ranges).<sup>23,24</sup> Orange and blue Solid lines, literature data for corresponding energies and HSPs for graphite (orange,<sup>25</sup> blue).<sup>6</sup> Black solid lines, HSPs for CB1(t). Red dashed and solid lines, HSPs for h-BN and graphene, respectively, estimated from our experimental data and literature data for carbon materials shown

Figure 6. continued

in (b). (b) Bottom graphs: Calculated RED (relative energy difference) numbers that reflect affinity of the solvents under investigation to carbon materials with different HSPs (CB, carbon black; CB(t), thermally treated carbon black; PC, petroleum coke). The lower the RED number the higher the affinity. HSPs for the carbon materials were taken from ref 26. Top graphs: the highest monolayer yields achieved in each solvent. In all graphs lines that connect the dots are guides for the eye.

and h-BN monolayers, and hence their HSPs may have similar values. The HSPs of the other carbons, which show the highest RED numbers for *i*-PrOH or the lowest RED numbers for DMF or 3-C<sub>8</sub>OH and C<sub>8</sub>OOH, are probably different from those of the monolayers. Among all the carbons, the distinctive feature of HSPs for CB1(t) is the largest contribution of the hydrogen bonding component, which is about two times higher than that of the polarity component, and these two components together constitute about 50% of all interactions. When putting the HSPs of CB1(t) on the graphs of monolayer yields *vs* HSP (Figure 6a, black lines), one can see that the  $d_H$  and  $d_p$  values are very close to those of the best solvents, whereas the  $d_D$  value is greater and beyond the  $d_D$  range of all the solvents. This suggests that the hydrogen bonding and polarity components of the graphene and h-BN monolayers are close to those of CB1(t), whereas their dispersion component may be lower. This allows us to estimate the HSP range for the monolayers at  $d_D = 17\text{--}20 \text{ MPa}^{0.5}$ ,  $d_p = 6\text{--}7 \text{ MPa}^{0.5}$ ,  $d_H = 12\text{--}14 \text{ MPa}^{0.5}$  and  $d_T = 22\text{--}25 \text{ MPa}^{0.5}$ . Again, this analysis suggests that the hydrogen bonding and dispersion interactions are primarily responsible for the strong affinity of both monolayer types to the solvents. The polarity interactions contribute about half of what the hydrogen bonding interactions do. This is consistent with the fact that DMF, which has  $d_H$  value close to that of the other solvents but a  $d_p$  value that is 2–4 times higher, is a less efficient solvent. DMF is the only aprotic solvent in the group that does not have hydrogen-bond-donor groups, which may result in the weaker interactions with the  $\pi$ -electron systems of the graphene and h-BN monolayers.

It is interesting to compare HSPs of the h-BN monolayers produced by exfoliation of h-BN/H<sub>3</sub>PO<sub>4</sub> with those of the sheets of exfoliated bare h-BN<sup>5</sup> (Figure 6a, red and blue dashed lines, respectively). Their total solubility parameters are close and the polarity components are similar but the monolayers derived from the intercalation compound have a considerably higher hydrogen bonding contribution (34% *vs* 22%) and lower dispersion contribution (50% *vs* 56%) to the total interaction with the solvents than the multilayer sheets obtained from bare h-BN (see SI pp 5–7 for details). Compared to the BN multilayer sheets, stronger hydrogen bonding interactions with solvents may be caused by the ultimate surface to volume ratio in the monolayer system where the Lewis acid and base sites of each atomic layer are available for interaction with the solvent molecules. However, some possible interactions with the residual H<sub>3</sub>PO<sub>4</sub> molecules that may remain adsorbed on the monolayer surface cannot be completely ruled out.

**Electronic Properties.** Current–Voltage (*I*–*V*) characteristics of a monolayer graphene sheet deposited on a p-doped Si(100) substrate were measured with Pt contacts in 2- and 4-probe setups under ambient conditions (see SI p 8 and Figure S8 for details). The *I*–*V* characteristics are linear, indicative of the ohmic Pt/graphene contacts. The resistivity of our

graphene-on-Si device ( $\rho = RWd/L$ , where  $R = DV/DI$ , measured resistance;  $W$ , width of the graphene sheet of  $5 \times 10^{-4}$  cm;  $L$ , distance between Pt contacts; and  $d$ , monolayer thickness of  $3 \times 10^{-8}$  cm) is  $(3 \div 6)10^{-2} \Omega\text{-cm}$ , which is 2–3 orders of magnitude higher than that of mechanically exfoliated graphene on a SiO<sub>2</sub> substrate.<sup>27–30</sup> This may be caused by extrinsic scattering in graphene due to adsorbed H<sub>2</sub>O/O<sub>2</sub> from air<sup>31</sup> and solvent/H<sub>3</sub>PO<sub>4</sub> occluded under and/or adsorbed on the graphene sheet. AFM images of the monolayer graphene sheets (Figure S8e) clearly show solvent occluded at the graphene/Si interface in the middle of the sheet that cannot be removed by many-day drying in vacuum. Also resistance of graphene devices can be higher for micron-scale intercontact distances,  $L$ ,<sup>27</sup> which is the case for our device.

Some perturbation effect of the Si substrate (or charged impurities associated with it) on the graphene  $\pi$ -electron system also cannot be ruled out. TERS spectra of the monolayer and few-layer graphene on p-doped Si substrate show a red shift of the G peak to 1601 cm<sup>-1</sup> and absence of the 2D peak (Figure S5c), while the Raman spectrum of a suspended agglomerate of our exfoliated mono- and few-layer graphene sheets show no noticeable changes compared to that of multilayer graphene<sup>32</sup> and starting graphite (Figure S5a,b). It has been shown that the 2D peak area is sensitive to the electronic inelastic scattering rate and that it decreases as the Fermi energy level moves away from the Dirac point.<sup>32</sup> The ratio of the intensities of the 2D and G peaks shows a strong dependence on doping and, at high n- and p-doping levels, the 2D peak can be completely suppressed.<sup>33–36</sup> Also, the red shift of the G peak suggests that our exfoliated graphene sheets on the p-doped Si substrate may be subject to p-doping.<sup>34–36</sup> This doping effect of the Si substrate, if it exists, might be enhanced by alkanol/H<sub>3</sub>PO<sub>4</sub> occluded at the Si/graphene interface. Control TERS experiments with a single layer of CVD graphene (CVD-SLG) grown on a Cu-substrate and then transferred on the same p-doped Si substrate (Figure S5d) show the presence of the 2D peak but the ratio of 2D/G peaks intensities,  $I_{2D}/I_G$ , is in the range of 1.3–0.7 (lexc = 488–633 nm) (Figure S5d,e), which is considerably lower than that of pristine CVD-SLG grown on a Cu-substrate ( $I_{2D}/I_G \sim 7.4$  at lexc = 488 nm) (Figure S5f). This fact suggests possible doping of CVD-graphene on Si,<sup>32–35</sup> which, however, is less pronounced compared to our graphene deposited from alkanol solution containing small amounts of H<sub>3</sub>PO<sub>4</sub>. The unintentional doping by the substrate is also a possibility and is mentioned in ref 37.

Despite the overall complexity of this system, we can conclude that the sp<sup>2</sup>  $\pi$ -electron system of graphene produced by exfoliation of graphite/H<sub>3</sub>PO<sub>4</sub> retains its integrity since the resistivity of our graphene monolayers is 1–2 orders of magnitude lower than that of reduced graphene oxide single sheets.<sup>38</sup>

## CONCLUSIONS

A high yield of atomically thin layers of graphene and h-BN can be achieved by exfoliation of first-stage phosphoric acid intercalation compounds of graphite and h-BN in medium polarity solvents, which have a large contribution of hydrogen bonding interactions to their total cohesive energy density. Solvents with hydrogen bond-donor atoms appear to be most effective, whereas aprotic solvents with a high contribution of polar interactions (e.g., DMF and DMSO) can morphologically damage the monolayers. The graphene and h-BN monolayers

obtained in this process are not very hydrophobic because the relative contributions of the dispersive and hydrogen bonding + polar interactions to their surface energy are approximately equal, whereas the polar interactions contribute about half of what the hydrogen bonding interactions do. These results suggest that a number of other organic solvents with ratios of solubility parameters close to those of the monolayers might be successfully used for exfoliation of acid-intercalated graphite and h-BN.

The intercalation/exfoliation process does not disrupt the  $sp^2$   $\pi$ -system of graphene and is gentle enough to allow the observation of monolayers that are tens of microns in their lateral dimensions. The integrity of the starting graphite and h-BN crystals is likely to determine the lateral size of the resulting monolayers. Solvents with longer alkyl chains are more efficient in stabilizing larger sheets in solutions of the exfoliated intercalation compounds.

## METHODS

First-stage graphite/ $H_3PO_4$  and h-BN/ $H_3PO_4$  intercalation compounds were prepared as described in our earlier papers.<sup>10,11</sup> Briefly, 24 mg (1 mmol) of cryo-milled graphite (CMG) or natural graphite powder (GAK-2, Ukraine, 325 mesh) and 25 mg (1 mmol) of h-BN (UK Abrasives Inc.) powders were mixed with 0.06 mL (1 mmol) and 0.12 mL (2 mmol), respectively, of 85 wt %  $H_3PO_4$ . The suspensions were spread on glass slides and kept at 120 °C thereafter with periodic XRD analysis. When the amounts of the intercalated phases in these graphite/ $H_3PO_4$  and h-BN/ $H_3PO_4$  systems reached relatively high values (Figure S1a) the samples were subjected to exfoliation in solvents.

About 1 mg of the graphite/ $H_3PO_4$  and h-BN/ $H_3PO_4$  samples that were kept at 120 °C was added to the solvent (1 mL) in a glass vial, which was preheated to the temperature of exfoliation and placed on a stirring plate. The suspensions were stirred at higher temperatures for 3 h and 45 h and then allowed to stand at room temperature for 40–45 days. Colloidal suspensions prepared in this way settle over a period of days but are completely resuspended by briefly stirring or shaking the vial.

For AFM and TERS analysis and electrical measurements, the suspensions were diluted with ethanol (1:100) and immediately dropcast onto a Si or sapphire substrate. The samples were dried under ambient conditions and then kept in vacuum at 40 °C.

The starting graphite and h-BN powders and graphite/ $H_3PO_4$  and h-BN/ $H_3PO_4$  intercalation compounds were characterized by X-ray powder diffraction, (XRD, Philips Empyrean, Cu  $K\alpha$  radiation) and field emission scanning electron microscopy (FESEM) (FEI NanoSEM 630 FESEM, low-vacuum mode, accelerating voltage 3 kV). The nanosheets after exfoliation were characterized by transmission electron microscopy (TEM, JEOL 1200 EXII, accelerating voltage 80 kV); FESEM (Zeiss Sigma VP-FESEM, InLens detector, accelerating voltage 3 kV), atomic force microscopy (AFM) with a Bruker Icon microscope in PeakForce QNM imaging mode using single crystal Si(100) substrates, and by micro-Raman spectroscopy (Renishaw inVia confocal microscope-based Raman spectrometer, laser 514.5 and 488 nm, laser spot  $\sim 1 \mu\text{m}$ ) and tip enhanced Raman spectroscopy (TERS, Horiba LabRam coupled to AIST-NT AFM, laser 633 and 532 nm). Raman spectra of h-BN sheets on Si were acquired with a Horiba LabRam HR Evolution UV Raman Spectrometer using a 74 $\times$  UV objective and a 290 nm wavelength laser excitation.

## ASSOCIATED CONTENT

### Supporting Information

The Supporting Information is available free of charge on the ACS Publications website at DOI: 10.1021/acsnano.7b01311.

X-ray diffraction patterns of intercalation compounds, temperature-dependent solvent cohesive energies, Raman spectra of exfoliated graphite/ $H_3PO_4$ , AFM images and data analysis, Hansen solubility parameters, and electrical measurements (PDF)

## AUTHOR INFORMATION

### Corresponding Author

\*E-mail: tem5@psu.edu.

### ORCID

Thomas E. Mallouk: 0000-0003-4599-4208

### Notes

The authors declare no competing financial interest.

<sup>†</sup>Deceased April 11, 2017.

## ACKNOWLEDGMENTS

AFM, TEM, SEM, TERS and XRD characterization was conducted in the research facilities of the Materials Research Institute and Huck Institute of Life Sciences of the Pennsylvania State University. We thank Haoyue Zhu for synthesis CVD-graphene samples. This work was supported by the U.S. Army Research Office MURI grant W911NF-11-1-0362.

## REFERENCES

- (1) Novoselov, K. S.; Fal'ko, V. I.; Colombo, L.; Gellert, P. R.; Schwab, M. G.; Kim, K. A Roadmap for Graphene. *Nature* **2012**, *490*, 192–200.
- (2) Zhi, C.; Bando, Y.; Tang, C.; Kuwahara, H.; Golberg, D. Large-Scale Fabrication of Boron Nitride Nanosheets and their Utilization in Polymeric Composites with Improved Thermal and Mechanical Properties. *Adv. Mater.* **2009**, *21*, 2889–2893.
- (3) Harrison, C.; Weaver, S.; Bertelsen, C.; Burgett, E.; Hertel, N.; Grulke, E. Polyethylene/Boron Nitride Composites for Space Radiation Shielding. *J. Appl. Polym. Sci.* **2008**, *109*, 2529–2538.
- (4) Hernandez, Y.; Nicolosi, V.; Lotya, M.; Blighe, F. M.; Sun, Z.; De, S.; McGovern, I. T.; Holland, B.; Byrne, M. Gun' High Yield Production of Graphene by Liquid-Phase Exfoliation of Graphite. *Nat. Nanotechnol.* **2008**, *3*, 563–568.
- (5) Coleman, J. N.; et al. Two-dimensional Nanosheets Produced by Liquid Exfoliation of Layered Materials. *Science* **2011**, *331*, 568–571.
- (6) Paton, K. R.; et al. Scalable Production of Large Quantities of Defect-free Few-layer Graphene by Shear Exfoliation in Liquids. *Nat. Mater.* **2014**, *13*, 624–630.
- (7) Huang, C.; Chen, C.; Ye, X.; Ye, W.; Hu, J.; Xu, C.; Qiu, X. Stable Colloidal Boron Nitride Nanosheet Dispersion and its Potential Application in Catalysis. *J. Mater. Chem. A* **2013**, *1*, 12192–12197.
- (8) Lin, Y.; Williams, T. V.; Xu, T. B.; Cao, W.; Elsayed-Ali, H. E.; Connell, J. W. Aqueous Dispersions of Few-Layered and Monolayered Hexagonal Boron Nitride Nanosheets from Sonication-Assisted Hydrolysis: Critical Role of Water. *J. Phys. Chem. C* **2011**, *115*, 2679–2685.
- (9) Badenhorst, H. Microstructure of Natural Graphite Flakes Revealed by Oxidation: Limitations of XRD and Raman Techniques for Crystallinity Estimates. *Carbon* **2014**, *66*, 674–690.
- (10) Kovtyukhova, N. I.; Wang, Y.; Berkdemir, A.; Cruz-Silva, R.; Terrones, M.; Crespi, V.; Mallouk, T. E. Non-oxidative Intercalation and Exfoliation of Graphite by Brønsted Acids. *Nat. Chem.* **2014**, *6*, 957–963.
- (11) Kovtyukhova, N. I.; Wang, Y.; Lv, R.; Terrones, M.; Crespi, V.; Mallouk, T. E. Reversible Intercalation of Hexagonal Boron Nitride with Brønsted Acids. *J. Am. Chem. Soc.* **2013**, *135*, 8372–8381.
- (12) Zacharia, R.; Ulbricht, H.; Hertel, T. Interlayer Cohesive Energy of Graphite from Thermal Desorption of Polyaromatic Hydrocarbons. *Phys. Rev. B: Condens. Matter Mater. Phys.* **2004**, *69*, 155406.

- (13) Bilinski, B. Free Energy Changes in Graphite/n-Hexane System. *Mater. Chem. Phys.* **1987**, *18*, 231–244.
- (14) Benedict, L. X.; Chopra, N. G.; Cohen, M. L.; Zettl, A.; Louie, S. G.; Crespi, V. H. Microscopic Determination of the Interlayer Binding Energy in Graphite. *Chem. Phys. Lett.* **1998**, *286*, 490–496.
- (15) Wang, W.; Dai, S.; Li, X.; Yang, J.; Srolovitz, D. J.; Zheng, Q. Measurement of the Cleavage Energy of Graphite. *Nat. Commun.* **2015**, *6*, 7853.
- (16) Roenbeck, M. R.; Wei, X.; Beese, A. M.; Naraghi, M.; Furmanchuk, A.; Pac, J. T.; Schatz, G. C.; Espinosa, H. D. *In Situ* Scanning Electron Microscope Peeling to Quantify Surface Energy between Multiwalled Carbon Nanotubes and Graphene. *ACS Nano* **2014**, *8*, 124–138.
- (17) Girifalco, L. A.; Lad, R. A. Energy of Cohesion, Compressibility, and the Potential Energy Functions of the Graphite System. *J. Chem. Phys.* **1956**, *25*, 693–697.
- (18) Kis, A.; Jensen, K.; Aloni, S.; Mickelson, W.; Zettl, A. Interlayer Forces and Ultralow Sliding Friction in Multiwalled Carbon Nanotubes. *Phys. Rev. Lett.* **2006**, *97*, 025501.
- (19) Liu, Z.; Liu, Z.; Zheng, Q. Interlayer Binding Energy of Graphite: A Mesoscopic Determination from Deformation. *Phys. Rev. B: Condens. Matter Mater. Phys.* **2012**, *85*, 205418.
- (20) Gobre, V. V.; Tkatchenko, A. Scaling Laws for van der Waals Interactions in Nanostructured Materials. *Nat. Commun.* **2013**, *4*, 2341.
- (21) Feicht, P.; Breu, J. Gas-phase Preparation of SO<sub>3</sub>-graphite: Host Exchange and Exfoliation. *Z. Anorg. Allg. Chem.* **2015**, *641*, 1093–1098.
- (22) Yang, T.; Berber, S.; Liu, J.-F.; Miller, G. P.; Tomanek, D. Self-assembly of Long-chain Alkenes and their Derivatives on Graphite. *J. Chem. Phys.* **2008**, *128*, 124709.
- (23) Rathod, N.; Hatzikiriakos, S. G. The Effect of Surface Energy of Boron Nitride on Polymer Processability. *Polym. Eng. Sci.* **2004**, *44*, 1543–1550.
- (24) Seth, M.; Hatzikiriakos, S. G.; Clere, T. M. Cross Melt Structure Elimination: The Role of Surface Energy of Boron Nitride Powders. *Polym. Eng. Sci.* **2002**, *42*, 743–752.
- (25) Wang, S.; Zhang, Y.; Abidi, N.; Cabrales, L. Wettability and Surface Free Energy of Graphene Films. *Langmuir* **2009**, *25*, 11078–11081.
- (26) Hansen, C. M. *Solubility Parameters: A User's Handbook*; CRC Press, 2007.
- (27) Baringhaus, J.; Ruan, M.; Edler, F.; Tejada, A.; Sicot, M.; Taleb-Ibrahimi, A.; Li, A.-P.; Jiang, Z.; Conrad, E. H.; Berger, C.; Tegenkamp, C.; de Heer, W. A. Exceptional Ballistic Transport in Epitaxial Graphene Nanoribbons. *Nature* **2014**, *506*, 349–354.
- (28) Chen, J.-H.; Jang, C.; Xiao, S.; Ishigami, M.; Fuhrer, M. Intrinsic and Extrinsic Performance Limits of Graphene Devices on SiO<sub>2</sub>. *Nat. Nanotechnol.* **2008**, *3*, 206–209.
- (29) Geim, A. K. Novoselov, The Rise of Graphene. *Nat. Mater.* **2007**, *6*, 183–191.
- (30) Lemme, M.; Echtermeyer, T. J.; Baus, M.; Kurz, H. A Graphene Field Effect Device. *IEEE Electron Device Lett.* **2007**, *28*, 282–284.
- (31) Mayorov, A. S.; Gorbachev, R. V.; Morozov, S. V.; Britnell, L.; Jalil, R.; Ponomarenko, L. A.; Blake, P.; Novoselov, K. S.; Watanabe, K.; Taniguchi, T.; Geim, A. K. Micrometer-scale Ballistic Transport in Encapsulated Graphene at Room Temperature. *Nano Lett.* **2011**, *11*, 2396–2399.
- (32) Ferrari, A.; Basko, D. Raman Spectroscopy as a Versatile Tool for Studying the Properties of Graphene. *Nat. Nanotechnol.* **2013**, *8*, 235–246.
- (33) Kalbac, M.; Reina-Cecco, A.; Farhat, H.; Kong, J.; Kavan, L.; Dresselhaus, M. S. The Influence of Strong Electron and Hole Doping on the Raman Intensity of CVD Graphene. *ACS Nano* **2010**, *10*, 6055–6063.
- (34) Das, A.; Pisana, S.; Chakraborty, B.; Piscanec, S.; Saha, S. K.; Waghmare, U. V.; Novoselov, K. S.; Krishnamurthy, H. R.; Geim, A. K.; Ferrari, A. C.; Sood, A. K. Monitoring Dopants by Raman Scattering in an Electrochemically Top-gated Graphene Transistor. *Nat. Nanotechnol.* **2008**, *3*, 210–215.
- (35) Dong, X.; Fu, D.; Fang, W.; Shi, Y.; Chen, P.; Li, L.-J. Doping Single-Layer Graphene with Aromatic Molecules. *Small* **2009**, *5*, 1422–1426.
- (36) Das, B.; Voggu, R.; Rout, C. S.; Rao, C. N. R. Changes in the Electronic Structure and Properties of Graphene Induced by Molecular Charge-transfer. *Chem. Commun.* **2008**, 5155–5157.
- (37) Ferrari, A. Raman Spectroscopy of Graphene and Graphite: Disorder, Electron-phonon Coupling, Doping and Nonadiabatic Effects. *Solid State Commun.* **2007**, *143*, 47–57.
- (38) Gomez-Navarro, C.; et al. Electronic Transport Properties of Individual Chemically Reduced Graphene Oxide Sheets. *Nano Lett.* **2007**, *7*, 3499–3503.